A biomass-assembled macro/meso-porous nano-scavenger for Hg ion trapping

Nan Nan Xia[1], Bingbing Zhang[2], Zi Hao Hu[1], Fangong Kong[1], Guomin Xu[2], Fei He[3]**

[1]State Key Laboratory of Biobased Material and Green Papermaking, Key Laboratory of Pulp & Paper Science and Technology of Shandong Province/Ministry of Education, Qilu University of Technology (Shandong Academy of Sciences), Jinan 250353, China

[2]National Engineering Research Center for Compounding and Modification of Polymer Materials, Guiyang, 550014, China

[3]School of Material Science and Engineering, University of Jinan, Jinan 250022, China

*Correspondence: pec.gmxu@gzu.edu.cn (G.X.); fei.he@seu.edu.cn (F.H.).

Characterization

Fourier transform infrared (FTIR) spectra (Bruker VERTEX70 FTIR, Karlsruhe, Germany) were recorded between 400 and 4000 cm^{-1} with a resolution of 4 cm^{-1} using a KBr pellet technique. The surface microstructures of samples were observed using a Regulus 8220 scanning electron microscope (SEM) (Hitachi High-Technologies Corporation). The transmission electron microscopy (TEM) was carried out on a JEM-2100 Plus microscope (JEOL, Japan) at an accelerating voltage of 200 kV. Surface analyses of LS-CTS-TA before and after Hg^{2+} adsorption were obtained by using X-Ray Photoelectron Spectroscopy (XPS) (Al Kα X-rays, ESCALAB250Xi, Thermo Fisher Scientific, USA). Peak positions were internally referenced to the C1s peak at 284.6 eV. Nitrogen adsorption/desorption isotherms were measured with a Micromeritics ASAP 2460 adsorptometer (Maike, Georgia, USA) using nitrogen as the adsorbate at 77 K. All samples were degassed at 150 °C for more than 10 h before analysis.

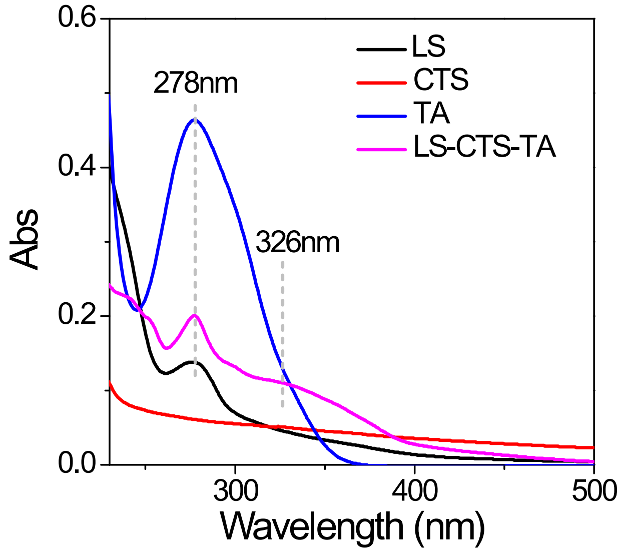

Figure S1 UV-Vis absorption of LS, CTS, TA and LS-CTS-TA before and after self-assembling.

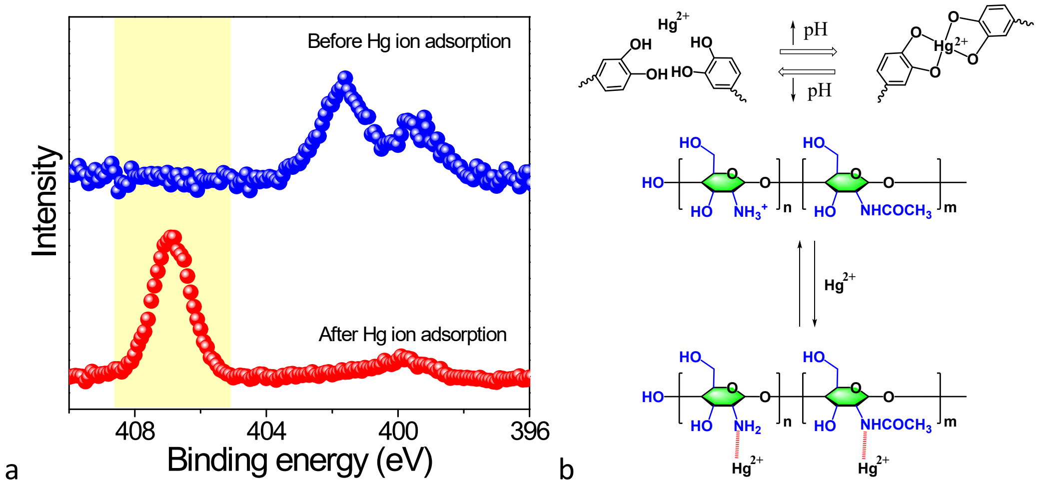

Figure S2 (a) N1s XPS spectra of LS-CTS-TA before and after adsorption of Hg ion. (b) Possible adsorption and desorption mechanism of Hg2+ over LS-CTS-TA. [1].

The catechol−metal coordination bonds possess reversible cleavage and formation capabilities at different pH (See the following Figure S2b), which has been demonstrated [1].

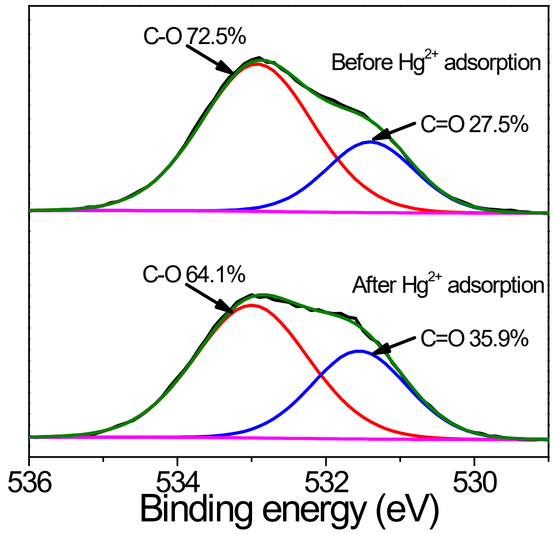

Figure S3 O1s XPS analysis of LS-CTS-TA before and after adsorption of Hg ion

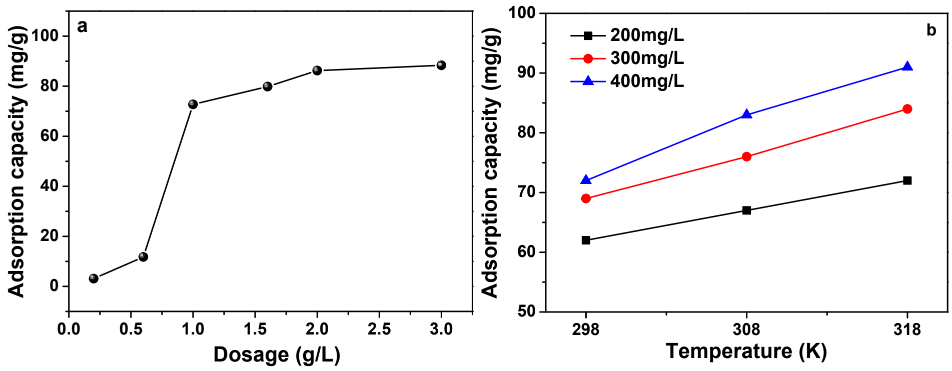

Figure S4 Adsorption capacity of LS-CTS-TA at different dosage (initial mercury concentration: 300mg/L, volume: 300mL, temperature: 25^{o}C, adsorption time: 2h, pH=7); (b) Adsorption capacity of LS-CTS-TA at different temperatures (initial mercury concentration: 300mg/L, volume: 300mL, adsorption time: 2h, pH=7).

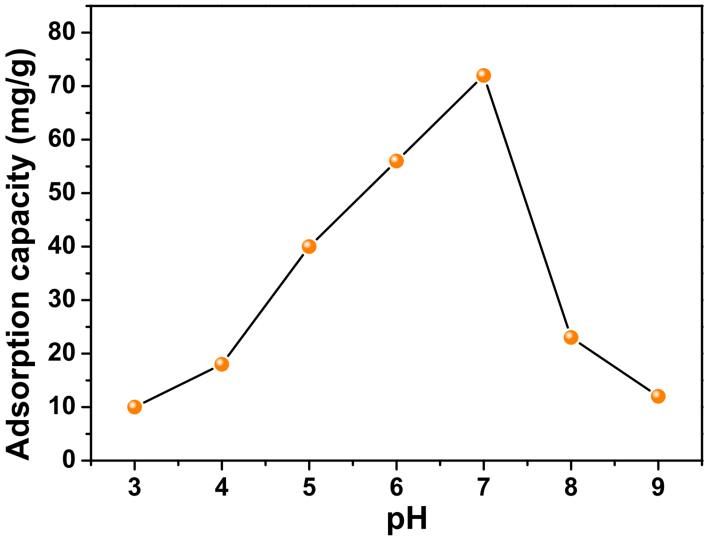

Figure S5 Adsorption capacity of LS-CTS-TA at different pHs (initial mercury concentration: 300mg/L, volume: 300mL, LS-CTS-TA: 0.3g, temperature: 25°C, adsorption time: 2h).

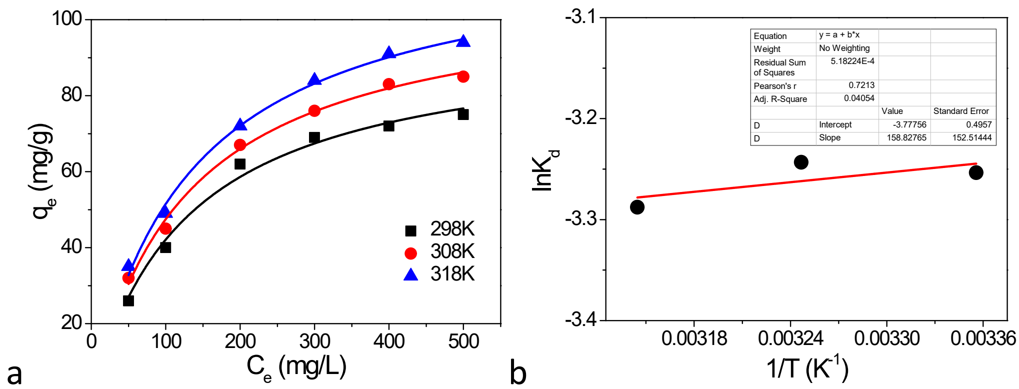

Figure S6 Adsorption isotherms of Hg ion on the LS-CTS-TA at different temperatures.

Thermodynamic parameters of Gibbs free energy (ΔG°, kJ/mol), enthalpy (ΔH°, kJ/mol) and entropy (ΔS°, kJ/mol/K) can be used to analyze the thermodynamics based on the following equations:

$$\Delta G^o = \Delta H^o - T\Delta S^o \qquad \text{Eq. s1}$$

$$lnK_d = \frac{\Delta S^o}{R} - \frac{\Delta H^o}{RT} \quad \text{Eq. s2}$$

Where, R is 8.314 J/(mol · K). K_d represented thermodynamic constant, the value of which was equal to that of the Langmuir equilibrium constant (ref: J. Chem. Eng. Data 2009, 54, 1981).

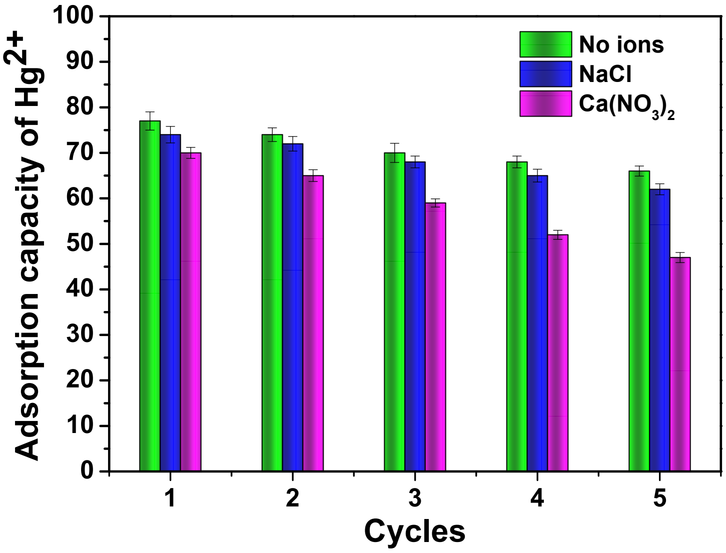

Figure S7 Adsorption performance of LS-CTS-TA under the interference of NaCl (50mg/L) or $Ca(NO_3)_2$ (50mg/L).

Table S1 Evaluated values of pseudo-first-order and pseudo-second-order rate constants and correlation coefficient for the adsorption of Hg^{2+} on LS-CTS-TA.

Sample	pseudo-first-order			pseudo-second-order			Intraparticle diffusion model		
	k_1 (min^{-1})	q_e (mg/g)	R^2	k_2 (kg/mol·min)	q_e (mg/g)	R^2	k_3	*C*	R^2
LS-CTS-TA	0.0316	77.46	0.9851	3.951×10^{-4}	90.68	0.9984	5.489	8.381	0.8962

Table S2 Langmuir and Freundlich isotherm constants of Hg^{2+} adsorption on LS-CTS-TA.

Material	Langmuir constants			Freundlich constants		
	K_L(L/mg)	q_m(mg/g)	R^2	1/n	K_F	R^2
LS-CTS-TA	0.00793	95.24	0.9935	0.46953	31.824	0.9447

Table S3 Hg^{2+} adsorption performances of different materials

Materials	pH	Temperature (°C)	Adsorption isotherm model	Q_m (mg/g)	References
Aulfur-modified pine-needle biochar	6.7	20	Freundlich	48.2	2
Carboxymethyl cellulose thiol-imprinted polymers	5.0	25	Langmuir	81.03	3
Cationic exchange resin of carboxyl banana stem	6.0	30	Langmuir	90.88	4a
Activated carbon made from sago waste	5.0	30	Langmuir	55.6	4b
Multi-functionalized corncob-derived biochar	6.0	25	Langmuir	14.1	4c
Dumbbell and flower shaped potato starch phosphate polymer	6.5	25	Langmuir	51.38	4d
Biomass of chlorella vulgaris	5.0	20	Lamgmuir	32.6	4e
Lignocellulosic materials	5.0	25	Lamgmuir	20	4f
Exhausted coffee waste	7	33	Langmuir	31.75	4g
Guanyl-modified cellulose	6	25	Langmuir	48	4h

Table S4 Thermodynamic parameters for Hg(II) adsorption over LS-CTS-TA

ΔH° (kJ/mol)	ΔS° (J/mol/K)	ΔG° (kJ/mol)		
		298 K	308 K	318 K
-1.32	-31.4	-8.04	-8.35	-8.66

Supporting references

1. Andersen A,; Krogsgaard M,; Birkedal H., Mussel-inspired self-healing double-cross-linked hydrogels by controlled combination of metal coordination and covalent cross-linking. *Biomacromolecules* **2017**, 19(5): 1402.

2. Jeon, C.; Solis, K. L.; An, H.-R.; Hong, Y.; Igalavithana, A. D.; Ok, Y. S., Sustainable removal of Hg(II) by sulfur-modified pine-needle biochar. *Journal of Hazardous Materials* **2020,** *388*, 122048.

3. Tarisai Velempini, K. P., Xavier Y. Mbianda, Omotayo A. Arotiba, Carboxymethyl cellulose thiol-imprinted polymers: Synthesis, characterization and selective Hg(II) adsorption. *Journal of Environmental Sciences* **2019,** *79*, 16.

4. (a) Anirudhan, T.; Senan, P.; Unnithan, M., Sorptive potential of a cationic exchange resin of carboxyl banana stem for mercury(II) from aqueous solutions. *Separation and Purification Technology* **2007,** *52* (3), 512-519; (b) Kadirvelu, K.; Kavipriya, M.; Karthika, C.; Vennilamani, N.; Pattabhi, S., Mercury (II) adsorption by activated carbon made from sago waste. *Carbon* **2004,** *42* (4), 745-752; (c) Faheem, F.; Bao, J.; Zheng, H.; Tufail, H.; Irshad, S.; Du, J., Adsorption-assisted decontamination of Hg(ii) from aqueous solution by multi-functionalized corncob-derived biochar. *RSC Advances* **2018,** *8* (67), 38425-38435; (d) Bashir, A.; Manzoor, T.; Malik, L. A.; Qureashi, A.; Pandith, A. H., Enhanced and selective adsorption of Zn(II), Pb(II), Cd(II), and Hg(II) Ions by a dumbbell- and flower-shaped potato starch phosphate polymer: A combined experimental and DFT calculation study. *ACS omega* **2020,** *5* (10), 4853-4867; (e) Solisio, C.; Al Arni, S.; Converti, A., Adsorption of inorganic mercury from aqueous solutions onto dry biomass of Chlorella vulgaris: kinetic and isotherm study. *Environmental technology* **2019,** *40* (5), 664-672; (f) Arias Arias, F. E.; Beneduci, A.; Chidichimo, F.; Furia, E.; Straface, S., Study of the adsorption of mercury (II) on lignocellulosic materials under static and dynamic conditions. *Chemosphere* **2017,** *180*, 11-23; (g) Mora Alvarez, N. M.; Pastrana, J. M.; Lagos, Y.; Lozada, J. J., Evaluation of mercury (Hg^{2+}) adsorption capacity using exhausted coffee waste. *Sustainable Chemistry and Pharmacy* **2018,** *10*, 60-70; (h) Kenawy, I. M.; Hafez, M. A. H.; Ismail, M. A.; Hashem, M. A., Adsorption of Cu(II), Cd(II), Hg(II), Pb(II) and Zn(II) from aqueous single metal solutions by guanyl-modified cellulose. *International journal of biological macromolecules* **2018,** *107* (Pt B), 1538-1549.